OMAE2021-62292

THE INFLUENCE OF LEADING-EDGE TUBERCLES ON THE SHEET CAVITATION DEVELOPMENT OF A BENCHMARK MARINE PROPELLER

Callum Stark
Department of Naval Architecture and Ocean Marine Engineering,
University of Strathclyde,
Glasgow, UK

Weichao Shi
Department of Naval Architecture and Ocean Marine Engineering,
University of Strathclyde,
Glasgow, UK

ABSTRACT

Cavitation is an undesirable phenomenon in the maritime industry as it causes damage to the propeller, degrading hydrodynamic performance and increasing the subsequent underwater radiated noise (URN). Therefore, mitigating cavitation on marine propellers is an important area of research in order to reduce carbon emissions emitted from the shipping industry and reduce the rate at which ocean ambient noise levels are increasing. The Humpback whale has provided inspiration to research in the fluid-structure interaction field due to the presence of leading-edge (LE) tubercles on the pectoral fins that allow it to perform acrobatic maneuvers to catch prey. This paper assesses the cavitation containment capability of the LE tubercles on a benchmark marine propeller in both heavy and light cavitating conditions using commercial code STAR-CCM+, unsteady incompressible Reynolds-averaged Navier Stokes (RANS) solver and the Schnerr-Sauer cavitation model to quantify the sheet cavitation present over a range of operating conditions. In summary, in heavy-cavitating conditions, a reduction in sheet cavitation with the inclusion of LE tubercles was observed to a maximum value of 2.75% in all operating conditions considered. A maximum improvement of 3.51% and 1.07% was predicted in propulsive thrust and hydrodynamic efficiency, respectively. In light cavitating conditions, although in some conditions a reduction in cavity volume was observed, this did not result in an improvement in hydrodynamic performance.

Keywords: Leading-edge tubercles, marine propeller, cavitation, biomimetics, CFD

1. INTRODUCTION

Cavitation is an ever-present issue within the maritime industry. It occurs due to a drop in local static pressure below the liquid saturation pressure and this can cause efficiency loss, hull/shaft vibrations, blade erosion and increased underwater radiated noise (URN) levels [1]. Cavitation creates increased levels of URN and carbon emissions due to performance degradation, two key issues within the maritime sector and further afield. Carbon emissions emitted from the shipping industry contribute to the rate of global warming, which influences every organism that resides on planet earth. Therefore, mitigating such affects is key to improving quality of life while also reducing fuel consumption and maintenance related costs for ship owners which is another key incentive for change. Also, URN has a detrimental impact on the acoustic marine environment utilised by numerous marine mammals to perform key biological functions. Due to this, the International Maritime Organization (IMO) published non-mandatory guidelines in 2014 to accelerate the reduction of ambient ocean noise levels [2]. Typically, the propulsion system generates most of the URN from marine vessels, especially in cavitating conditions. Therefore, reducing cavitation is key to reduce URN, increase hydrodynamic efficiency and the propeller life at sea which will; reduce carbon emissions emitted from the shipping industry, improve the acoustic marine environment and reduce the associated maintenance costs of cavitation-induced damage on the propeller. The awareness of the maritime industry of such issues has driven the development of various technologies such as the decelerating duct, propeller boss cap fins (PBCF), the Kappel and Contracted and Loaded Tip (CLT) propeller in order to suppress different cavitation mechanisms [3]. Interestingly, the end plate modifications on the Kappel and CLT propellers are inspired by nature, resembling winglets, a very popular device on aircraft wings to reduce tip vortices. Biomimetic concepts

such as this have resulted in great benefits to the performance of many different devices.

Ironically, a marine mammal that is affected by the by-products of marine vessels, is the inspiration behind this research. The Humpback whale is an incredible marine mammal, performing agile movements to capture prey and this is made possible with the small bumps on the leading-edge of the pectoral fin, known as leading-edge (LE) tubercles. This concept is the focus of many applications such as the aerofoil and the tidal turbine, where it has shown to improve hydro/aerodynamic performance in stall conditions, reduce noise and contain cavitation. This is due to the counter-rotating vortices that are produced by the sinusoidal pattern, creating a high-low pressure pattern from peak to trough, energising the boundary and encouraging flow attachment which would typically not be possible without such a feature [4].

The hydrodynamic benefits of LE tubercles were first explored by Watts and Fish using the panel method on a NACA aerofoil profile [5]. Miklosovic et al [6] conducted an experimental investigation using a wind tunnel, to investigate LE tubercles on a scale Humpback whale flipper model. The measurements showed that the stall angle of the flipper was delayed by 40%. Marine control surfaces such as rudders have also been the benefactors of LE tubercle research. Johari et al [7] explored the geometrical parameters of the sinusoidal LE tubercle pattern, wavelength and amplitude on hydrofoil performance in a water tunnel. It was concluded that in the pre-stall condition, the inclusion of LE tubercles degraded the performance of the aerofoil by reducing lift and increasing drag. But, in the post-stall condition, the inclusion of the LE tubercles resulted in a 50% increase in lift with a negligible drag penalty. It was noted that the performance of the LE tubercle aerofoil was more sensitive to amplitude than to wavelength. Weber et al [8] used experimental methods to investigate the effect of LE tubercles on the lift, drag and cavitation onset operating at low Reynold's numbers. It was concluded that the inclusion of LE tubercles accelerated the onset of cavitation. However, the distribution of cavitation was altered, compartmentalising the cloud cavitation into slots in the troughs. Therefore, it was inferred that under heavy-cavitating conditions that the rudder with LE tubercles would provide superior hydrodynamic performance due to this phenomenon.

Since the above-mentioned fundamental studies, the concept has been researched on rotating machinery such as the tidal turbine and more recently, the marine propeller. Shi et al [9-11] established the concept onto the tidal turbines. An in-depth numerical and experimental study was conducted into the feasibility of LE tubercles on such a device. The work showed an improvement in power coefficient at low tip speed ratios, containment of cavitation and reduction of URN in some operating conditions. It was found that the inclusion of LE tubercles resulted in an earlier inception of cavitation, but in heavier cavitating conditions the cavitation was restricted to the troughs of the tubercles, similar findings to Weber et al [8].

Additionally, the influence of LE tubercles on marine propellers has been investigated [12,13]. Ibrahim and New [12] conducted a numerical investigation using CFD to conclude that LE tubercles can improve the total raw power output of the propulsive device, although an increase in torque results in a lower propulsive efficiency. Charalambous and Eames [13] used numerical methods to show at a single operating condition, sheet cavitation is influenced by LE tubercles. However, the understanding of the influence of LE tubercles on marine propeller hydrodynamic performance in cavitating conditions and the development of sheet cavitation on the blade surface is still in its infancy. This study aims to further the state-of-the-art by addressing this knowledge gap.

In summary, LE tubercles have shown the potential to improve hydrodynamic performance in heavy-cavitating conditions for different marine devices, but this has not been studied in-depth on an application such as the marine propeller. Therefore, this paper aims to contribute to the state-of-the-art by assessing the cavitation containment capability of LE tubercles on a benchmark marine propeller in both heavy and light cavitating conditions over a range of operating conditions. This was accomplished by using commercial code STAR CCM+, the incompressible Reynolds-averaged Navier Stokes (RANS) solver and the Schnerr-Sauer cavitation model to describe the sheet cavitation present.

2. NUMERICAL APPROACH
2.1 Hydrodynamic Solution

The hydrodynamic flow field was solved using the implicit unsteady incompressible RANS solver from commercial code STAR-CCM+, which has been used extensively for a wide array of maritime problems amongst the engineering community. Firstly, a moving reference frame (MRF) approach with steady RANS was used to simulate the propeller open-water performance to compare with the experimental test. The steady MRF method is a time-averaged approach where the propeller is fixed, and the rotating region adopts a local frame of reference. To obtain the open-water curve, the propeller rotational rate was fixed at 15rps, while the advance velocity V_A was varied. Then, the Rigid Body Motion (RBM) method with unsteady RANS was implemented to perform the transient analysis with the propeller moving with a fixed displacement per time step. Momentum equations were discretised using the second-order scheme. Temporal discretization was also done using a second-order scheme. In both methodologies, the SST k-omega turbulence model was used. The time-step used was 1 degree of rotation per time-step and the propeller ran for approximately 20 revolutions.

2.2 Cavitation Model

In STAR CCM+, the multiphase flow was modelled using the volume of fluid (VOF) model and the cavitation behaviour was described using the Schnerr-Sauer model. The Schnerr-Sauer model is based on the reduced Rayleigh-Plesset equation, and neglects the influence of bubble growth acceleration, viscous effects, and surface tension. Nonetheless, this model has provided good agreement with experimental sheet cavitation observations [14].

The cavitation number, $Cav_{0.7r}$, can be described in Eqn. 1.

$$Cav_{0.7r} = \frac{P_{0.7r} - P_v}{\frac{1}{2}\rho(V_A^2 + (0.7\omega r)^2)} \quad (1)$$

where $P_{0.7r}$ is the static pressure at the upper 0.7 radius of the propeller including the Atmospheric pressure, Pa; Pv is the vapour pressure of the water, Pa;ω is the rotational speed, rad/s; ρ is the water density, kg/m^3; V_A is the advance velocity, m/s; r is the propeller radius, m.

3. TEST CASE

3.1 Overview

The baseline labelled 'BASE' and LE tubercle marine propeller geometry labelled 'TUB' can be shown in Fig. 1. The baseline geometry was based on the standard five-bladed Wageningen B-screw series propeller [1]. The main geometrical parameters can be found in Tab. 1.

a)   BASE   b)   TUB

FIGURE 1: BASE AND TUB PROPELLER GEOMETRY

TABLE 1: GEOMETRICAL PARAMETERS OF REFERENCE PROPELLER

Variable (Propeller)	Unit
Type	B-series (modified)
Blade Number	5
Expanded Area Ratio (EAR)	0.6
Pitch-diameter Ratio (P/D)	1.2
Diameter, D	0.3m
Rake	0º

In this study, the reference propeller is based on a B-series propeller design; however, due to the variation of the propeller blade section along the radius, to design a tubercle that suits all sections is paramount. Therefore, the propeller is simplified using one identical foil section (NACA0012) throughout the blade sections. Based on a previously developed 2D tubercle foil,

the NACA0012 is optimised with two ranges of tubercle designs, wavelength, λ=0.3c&0.5c and height, H=0.1c, where c is the foil chord length as shown in Fig. 2 and compared to experimental data at Reynolds number = 5x10^6 acquired from [15]. It can be seen the design with λ=0.5c and H=0.1c has a better performance over the range of angles of attack. Therefore, the design has continued to be used for the propeller design and in this study the optimised height to wavelength ratio is adopted.
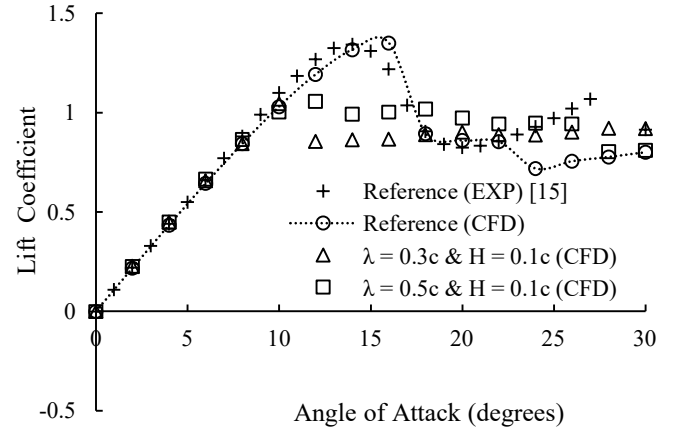

FIGURE 2: NACA 0012 TUBERCLE OPTIMISATION PLOT

3.2 Computational Domain

The computational domain is as shown in Fig. 3. The inlet was described as velocity inlet, where the velocity was selected as the advance velocity, V_A (m/s) and was varied to vary the advance ratio, J. The outlet was defined as pressure outlet and symmetry plane on the cylindrical far-field face. The rotating region was separated from the static region, to rotate the flow. The inlet was located 4D, the outlet was located 10D and symmetry planes located at 2D from the propeller centre.
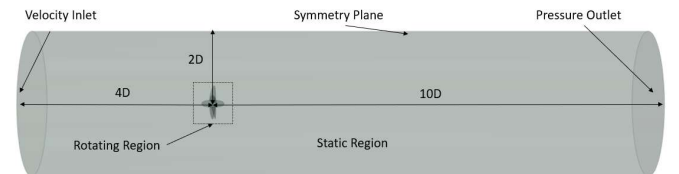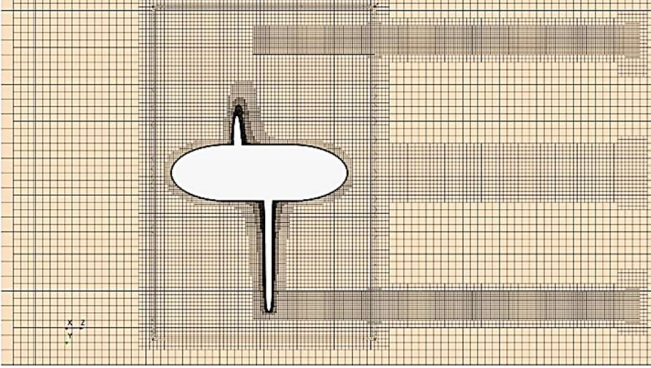

FIGURE 3: THE COMPUTATIONAL DOMAIN

3.3 Mesh Generation

Unstructured hexahedral mesh was used, with the final mesh containing approximately 13 million cells. Volumetric controls in the downstream region were used to resolve the tip and hub vortex structure with a higher resolution. The average y+ value of the boundary layer was maintained below 1, with a maximum of 2.7 present at the blade leading-edge. This was done by applying a prism layer mesh to resolve the boundary layer. An interface prism layer was inserted between rotating and static regions to ensure mesh alignment between the interfaces. The blade surface mesh was uniform across the full blade area.

The volume mesh can be shown in Fig. 4 and the blade surface mesh of both geometries in Fig. 5.

FIGURE 4: A CUT PLANE ILLUSTRATING THE VOLUME MESH OF DOMAIN

FIGURE 5: THE BASE AND TUB BLADE SURFACE MESH

4.   VERIFICATION AND VALIDATION
4.1 Performance Coefficients

The performance of the marine propeller follows the traditional open-water curve characteristics. The variables, propeller thrust, K_{TP} torque K_Q and efficiency, ETA can be described in Eqns. 2, 3 and 4, respectively. Advance ratio, J, can be defined in Eqn. 5.

$$K_{TP} = \frac{T}{\rho n^2 D^4} \qquad (2)$$

$$K_Q = \frac{Q}{\rho n^2 D^5} \qquad (3)$$

$$ETA = \frac{K_{TP}J}{2\pi K_Q} \qquad (4)$$

$$J = \frac{V_A}{nD} \qquad (5)$$

Advance ratio, J, is defined by advance velocity V_A (m/s), n, rotation rate (rps) and propeller diameter D (m). T is propeller thrust (N), Q is propeller torque (Nm) and ρ, is density (kg/m^3).

4.2 Mesh Convergence

A verification study was conducted to determine the uncertainty of the numerical simulations. This was completed using the grid convergence (GCI) method. The full methodology implemented in this study was defined by Celik et al [16] and can be found within. The total thrust and torque coefficient were selected as the integral variable at advance ratio, J=0.6. The tabulated results can be shown in Tab. 2.

The difference between the solution scalars (ε) should be determined by Eqn. 6.

$$\varepsilon_{21} = \varphi_2 - \varphi_1, \; \varepsilon_{32} = \varphi_3 - \varphi_2, \qquad (6)$$

where, φ_1, φ_2 and φ_3 represent the results using fine, medium and coarse mesh grids, respectively. The ratio of solution scalars is used to calculate the convergence condition by Eqn. 7.

$$R = \frac{\varepsilon_{21}}{\varepsilon_{32}} \qquad (7)$$

Solution type is determined with respect to the convergence condition, R: 1. oscillatory convergence, $-1<R<0$; 2. monotonic convergence $0<R<1$; 3. oscillatory divergence $R<-1$; and 4. monotonic divergence, $R>1$, If R is found as in case 2, the procedure can be directly employed. GCI index is calculated by the following in Eqn. 8:

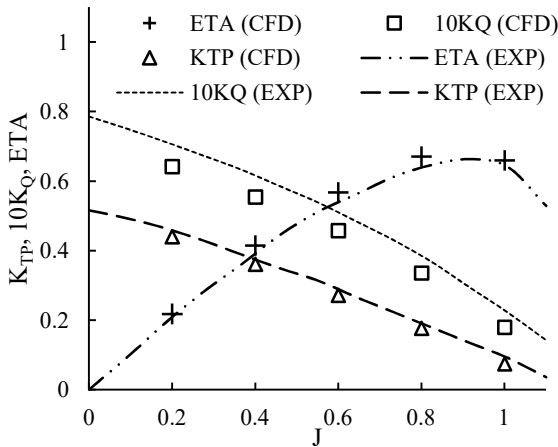$$GCI_{fine}{}^{21} = \frac{1.25 e_a{}^{21}}{r_{21}{}^{p} - 1} \qquad (8)$$

Here, p is apparent order, e_a is an approximate relative error. Detailed information about the verification procedure can be found in [16]. Results obtained for the thrust and torque coefficient and uncertainty level for both propeller geometries at J = 0.6 are given in Tab. 2. The convergence condition (R) was between 0 and 1 (monotonic convergence). In addition, a grid sensitivity study was conducted for BASE geometry at J = 0.6, $CAV_{0.7r}$ =0.47 to quantify the uncertainty in the cavitation volume when cavitation was present within the unsteady simulations. Monotonic convergence was observed, and the uncertainty error, GCI$_{FINE}$ was approximately 1%. As a result of the uncertainty studies, the fine mesh was selected.

TABLE 2: UNCERTAINTY RESULT FOR K_{TP} AND $10K_Q$

		φ_1	φ_2	φ_3	R	%GCI$_{FINE}$
BASE	K_{TP}	0.272	0.273	0.278	0.26	0.33
	$10K_Q$	0.457	0.461	0.475	0.29	0.70
TUB	K_{TP}	0.273	0.274	0.278	0.31	0.37
	$10K_Q$	0.462	0.466	0.481	0.27	0.62

4.3 Hydrodynamic Validation with Experimental Test

The numerical simulated open-water (OPW) performance curve characteristics were compared to the experimental tests of the baseline design at CNR-INM and can be shown in Fig 6.

FIGURE 6: VALIDATION OF OPW CURVE WITH EXPERIMENTAL TEST

As can be seen, comparing the numerical results with the experimental test conducted at CNR-INM, it shows good agreement between the open-water characteristics of thrust, torque and propulsive efficiency.
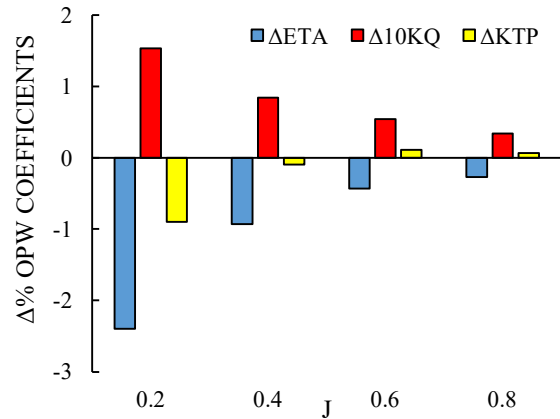
5. NON-CAVITATING HYDRODYNAMIC PERFORMANCE RESULTS AND ANALYSIS

Figure. 7 shows the effect on the propulsive efficiency, torque and thrust at various advance ratios when comparing the tubercle 'TUB' marine propeller to the 'BASE' propeller in non-cavitating conditions. The time-averaged non-cavitating performance characteristics were obtained using the RBM method. Generally, the TUB propeller provided an increase in torque resulting in a lower propulsive efficiency, with a maximum reduction of 2.39% in the heaviest-loaded condition considered. A similar general trend was found by [12] where the overall efficiency did not improve due to the increase in torque. However, the increase in torque and reduction in propulsive efficiency becomes less prominent with reduced blade

loading/increasing J. Table. 3 shows the change in key OPW variables.

TABLE 3: COMPARISON IN KEY VARIABLES, PROPELLER THRUST, TORQUE AND EFFICIENCY IN NON-CAVITATING CONDITIONS

J	ΔK_{TP} %	$\Delta 10K_Q$ %	ΔETA %
0.2	-0.90	1.53	-2.39
0.4	-0.10	0.84	-0.93
0.6	0.11	0.54	-0.43
0.8	0.07	0.34	-0.27

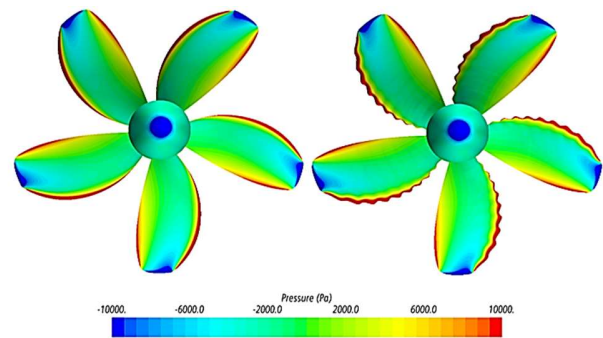**FIGURE 7:** Δ% IN OPW VARIABLES VS. J FOR THE TUB PROPELLER WHEN COMPARED TO THE BASE IN NON-CAVITATING CONDITIONS.

6. NON-CAVITATING HYDRODYNAMIC FLOW-FIELD RESULTS AND ANALYSIS
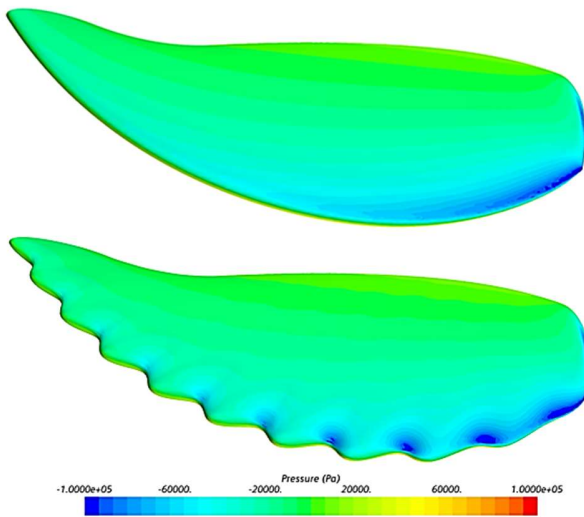
6.1 Surface Pressure Distribution

Figure. 8 shows the pressure side of the BASE and TUB propeller geometry at J = 0.6. As can be seen there is no appreciable difference between the BASE and TUB propeller on the pressure side of the blades at this operating condition.

FIGURE 8: PRESSURE SIDE OF BASE AND TUB PROPELLER GEOMETRY AT J = 0.6
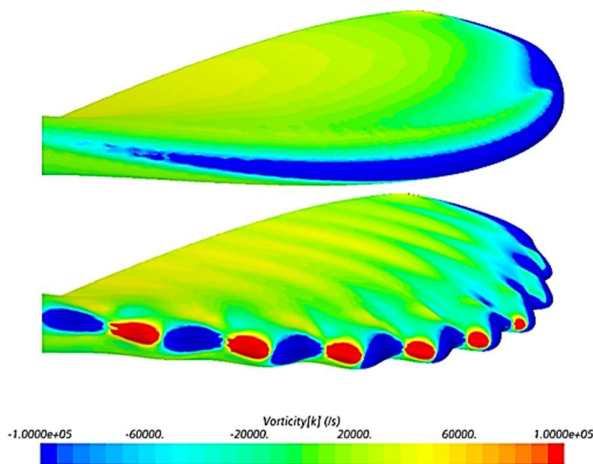
Figure. 9 shows the suction side of the BASE and TUB propeller geometry at J = 0.6. Note the high-low pressure pattern occurring on the LE of the TUB blade when compared to the low-pressure strip on the LE of the BASE propeller blade. In addition, the LE tubercles induce lower pressure regions on the blade that were not present on the smooth leading edge, particularly nearer the blade root.

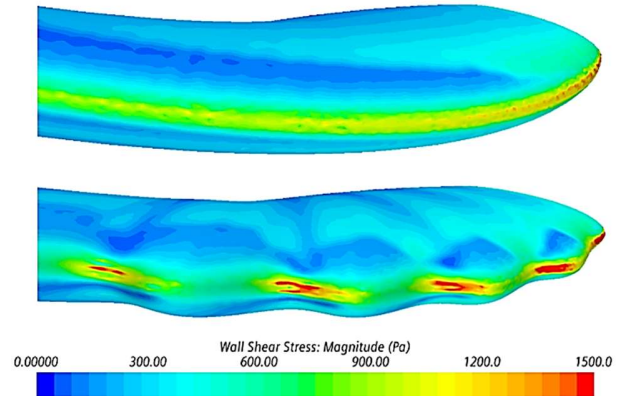**FIGURE 9:** SUCTION SIDE OF BASE AND TUB GEOMETRY AT J = 0.6

6.2 Surface Streamwise Vorticity and Wall Shear Stress Distribution

Figure. 10 shows the distribution of the streamwise vorticity on a single BASE and TUB propeller blade at J = 0.6. As can be seen, the TUB propeller creates the counter-rotating vortices, a fundamental mechanism produced by the tubercle concept, becoming less distinct nearer the blade tip.

FIGURE 10: STREAMWISE VORTICITY DISTRIBUTION OF BASE AND TUB PROPELLER GEOMETRY AT J = 0.6
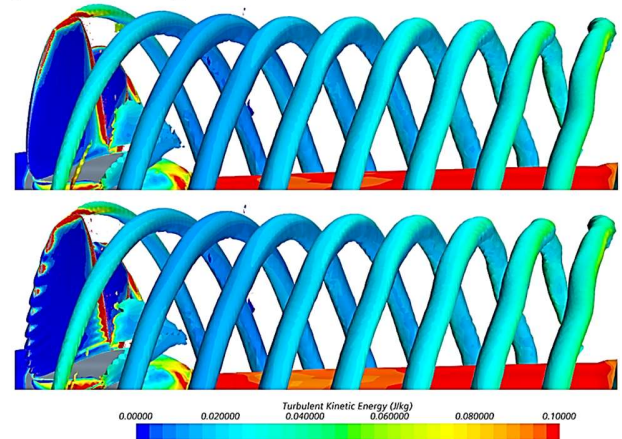
Figure. 11 shows the wall shear stress distribution along the blade of the BASE and TUB propeller geometry at J = 0.6. As can be seen, the inclusion of the LE tubercles results in a higher wall shear stress in the trough-peak section that faces the root of the TUB propeller blade when compared to the BASE propeller blade at the same position.

FIGURE 11: WALL SHEAR STRESS ILLUSTRATION OF BASE AND TUB PROPELLER GEOMETRY AT J = 0.6, RESPECTIVELY.

6.3 Vorticity Wake Flow Distribution

Figure. 12 shows the Q-criterion iso-surface coloured with turbulent kinetic energy (TKE) of BASE and TUB propeller geometry at J = 0.6, respectively. The tip vortex in the propeller slipstream can be clearly visualized for both propellers. Although previous reduction in tip vortex has been observed with the inclusion of tubercles on rotating devices [10], this was not observed in this case most likely due to the geometrical parameters not being prominent enough near the tip for this particular configuration.

FIGURE 12: Q-CRITERION α = 1000/S^2, COLOURED BY TKE FOR BASE (TOP) AND TUB (BOTTOM) PROPELLER GEOMETRY AT J = 0.6
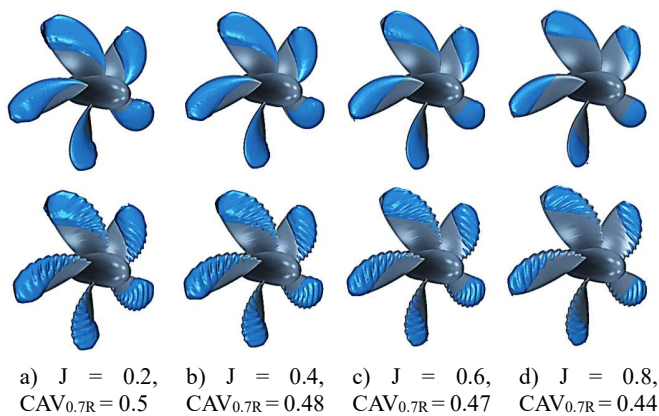
7. SHEET CAVITATION RESULTS AND ANALYSIS

The sheet cavitation was predicted over operating conditions J = 0.2, 0.4, 0.6 and 0.8 and at a low cavitation number ranging from 0.44-0.55 and a higher cavitation number ranging from 1.31-1.5. This was done by selecting two reference pressures and applying them both to a variety of advance ratios. The key performance variables and cavity volume changes with the addition of LE tubercles can be shown in Tab. 4.

TABLE 4: COMPARISON IN KEY VARIABLES, PROPELLER THRUST, PROPULSIVE EFFICIENCY AND CAVITY VOLUME IN CAVITATING CONDITIONS.

J	$CAV_{0.7r}$	ΔK_{TP} %	ΔETA %	ΔVOL %
0.2	0.50	3.51	1.07	-0.06
0.4	0.48	2.80	0.86	-1.98
0.6	0.47	1.41	0.42	-2.53
0.8	0.44	1.09	0.80	-2.75
0.2	1.51	-0.94	-0.92	-4.56
0.4	1.47	-0.94	-0.96	-11.03
0.6	1.42	-0.24	-0.62	19.00
0.8	1.35	-	-	-

Tab. 4 shows the results from the cavitation investigation. As can be seen, the LE tubercles are superior in the heavy-cavitating conditions, with an improvement in propeller thrust and efficiency due to the reduction in sheet cavitation volume at all operating conditions studied. Figure. 13 shows the vapour fraction iso-surface (α =0.5) for the heavy-cavitating operating conditions investigated. The maximum performance enhancement was observed at J = 0.2, $CAV_{0.7r}$ = 0.5, with an improvement in propeller thrust of 3.51% and an improvement of efficiency of 1.07%. The cavitation volume change at this condition due to the inclusion of tubercles is minimal, therefore the distribution of sheet cavitation influences the resulting effect on the thrust and efficiency of the propeller where some cavitation is redistributed from the mid-section of the blade to the root, similar to that shown in Fig. 14.
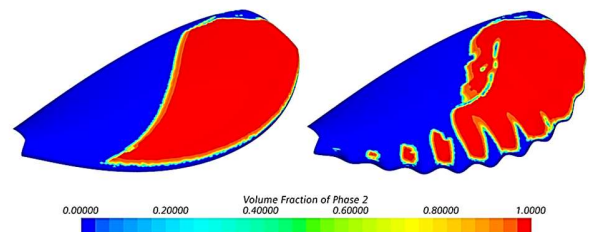

a) J = 0.2, $CAV_{0.7R}$ = 0.5   b) J = 0.4, $CAV_{0.7R}$ = 0.48   c) J = 0.6, $CAV_{0.7R}$ = 0.47   d) J = 0.8, $CAV_{0.7R}$ = 0.44

FIGURE 13: BASE (TOP) AND TUB (BOTTOM) PROPELLERS AT $CAV_{0.7R}$=0.44-0.5 AND J=0.2-0.8. ISO-SURFACE (α = 0.5) OF VAPOUR FRACTION.
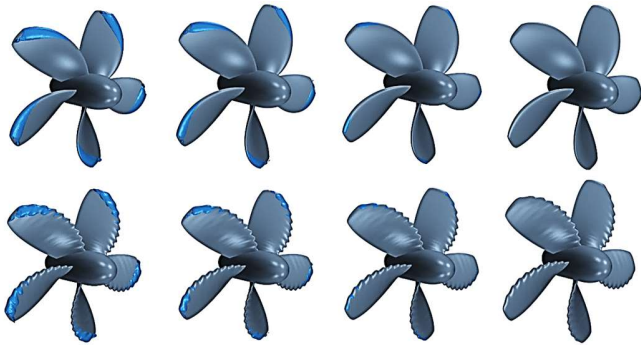
The LE tubercles effect on the development is shown clearly, the high-low pressure pattern on the LE of the blade creating a wavy, ridge-like sheet cavitation pattern, compared to the bulky block-like pattern produced by the baseline design. This is believed to be due to the streamwise counter-rotating vortices produced by the LE tubercles which disrupt the pressure distributions along the leading-edge of the blade. This can be further confirmed with the vapour fraction plotted on the BASE and TUB propellers as shown in Fig. 14, where the higher pressure regions behind the peak of the tubercles create a fence-like sheet cavitation pattern, compartmentalising the cavitation to the troughs, particularly near the root of the blade at this condition.

Figure. 15 shows the vapour fraction iso-surface (α = 0.5) to represent the cavitation volume at light cavitating conditions. At these conditions, there was a reduction in propulsive efficiency and thrust in all operating conditions. Although a reduction in cavity volume was observed at some conditions, the efficiency did not improve.

The reduction in thrust and propulsive efficiency despite the reduction in cavity volume is likely due to minimal thrust degradation predicted due to the presence of light cavitation when compared to no cavitation present. In addition to this reason, another reason could be due to the cavitation volume being induced further to the blade mid-section than near the tip by the tubercles, where a larger proportion of thrust is likely to be generated. At the operating condition where cavitation is the lightest, J =0.6, $CAV_{0.7r}$ = 1.42, the inclusion of the LE tubercles results in an increase in cavity volume, this is likely due to the tubercles inducing lower pressure regions in areas of the blade LE than the baseline design would and therefore, producing cavitation in an area that would have not been originally produced by the baseline design at the same operating condition. This can be further confirmed by plotting the vapour fraction on both the BASE and TUB blades at two conditions of interest as shown in Fig. 16. The cavitation can be seen to be present in the low-pressure trough regions when compared to no cavitation being present in the higher-pressure peak regions creating a fencing pattern compared to a continuous length of cavitation along the BASE blade. Due to this, sheet cavitation can be seen to be distributed further down the blade from the tip for the TUB blade compared to the BASE.

FIGURE 14: VAPOUR FRACTION (VOLUME FRACTION OF PHASE 2) AT J = 0.6, $CAV_{0.7R}$ = 0.47 FOR BASE (LEFT) AND TUB (RIGHT) PROPELLERS

| a) J = 0.2, $CAV_{0.7R}$ = 1.51 | b) J = 0.4, $CAV_{0.7R}$ = 1.47 | c) J = 0.6, $CAV_{0.7R}$ = 1.42 | d) J = 0.8, $CAV_{0.7R}$ = 1.35 |

FIGURE 15: BASE (TOP) AND TUB (BOTTOM) PROPELLERS AT $CAV_{0.7R}$=1.35-1.51 AND J=0.2-0.8. ISO-SURFACE (α = 0.5) OF VAPOUR FRACTION.
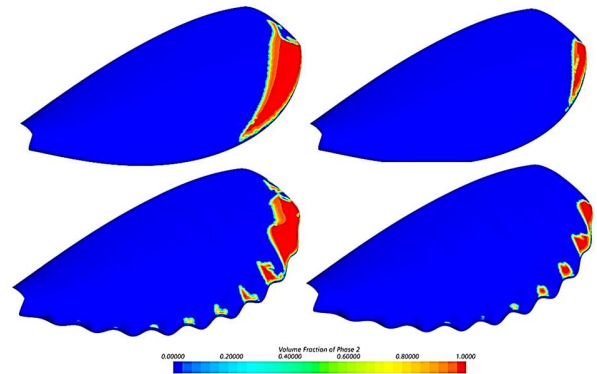
8. CONCLUDING REMARKS

In conclusion, in heavy-cavitating conditions this geometrical configuration of tubercle creates a fence-like sheet cavitation pattern on the propeller blades, which can reduce and redistribute the cavity volume and improve propulsive thrust and efficiency.

ACKNOWLEDGEMENTS

REFERENCES

[1]   Carlton, J. (2018). Marine propellers and propulsion. Butterworth-Heinemann.

[2]   IMO, M. (2014). Guidelines for the reduction of underwater noise from commercial shipping to address adverse impacts on marine life.

[3]   Ebrahimi, A., Razaghian, A. H., Seif, M. S., Zahedi, F., & Nouri-Borujerdi, A. (2019). A comprehensive study on noise reduction methods of marine propellers and design procedures. Applied Acoustics, 150, 55-69.

[4]   New, D. T., & Ng, B. F. (2020). Flow Control Through Bio-inspired Leading-Edge Tubercles.

[5]   Watts, P., & Fish, F. E. (2001, August). The influence of passive, leading edge tubercles on wing performance. In Proc 12th Internat Symp Unmanned Untethered Submersible Tech. Durham.

[6]   Miklosovic, D. S., Murray, M. M., Howle, L. E., & Fish, F. E. (2004). Leading-edge tubercles delay stall on humpback whale (Megaptera novaeangliae) flippers. Physics of fluids, 16(5), L39-L42.

[7]   Johari, H., Henoch, C., Custodio, D., & Levshin, A.

FIGURE 16: VAPOUR FRACTION (VOLUME FRACTION OF PHASE 2) AT J = 0.4, $CAV_{0.7R}$ = 1.47 (LEFT) AND FOR J = 0.6, $CAV_{0.7R}$ = 1.42 (RIGHT) FOR BASE (TOP) AND TUB (BOTTOM) PROPELLERS

       (2007). Effects of leading-edge protuberances on airfoil performance. AIAA journal, 45(11), 2634-2642.

[8]   Weber, P. W., Howle, L. E., & Murray, M. M. (2010). Lift, drag, and cavitation onset on rudders with leading-edge tubercles. Marine technology, 47(1), 27-36.

[9]   Shi, W., Atlar, M., Norman, R., Aktas, B., & Turkmen, S. (2016). Numerical optimization and experimental validation for a tidal turbine blade with leading-edge tubercles. Renewable Energy, 96, 42-55.

[10]   Shi, W., Atlar, M., Rosli, R., Aktas, B., & Norman, R. (2016). Cavitation observations and noise measurements of horizontal axis tidal turbines with biomimetic blade leading-edge designs. Ocean engineering, 121, 143-155.

[11]   Shi, W., Atlar, M., & Norman, R. (2017). Detailed flow measurement of the field around tidal turbines with and without biomimetic leading-edge tubercles. Renewable Energy, 111, 688-707.

[12]   Ibrahim, I. H., & New, T. H. (2015, June). Tubercle modifications in marine propeller blades. In 10th Pacific symposium on flow visualization and image processing. Naples, Italy (pp. 15-18).

[13]   Charalambous, N., & Eames, I. (2019, May). A computational analysis of a marine propeller with tubercle and its contribution in reducing sheet cavitation. Sixth International Symposiums on Marine Propulsors.

[14]   Sezen, S., Atlar, M., Fitzsimmons, P., Sasaki, N., Tani, G., Yilmaz, N., & Aktas, B. (2020). Numerical cavitation noise prediction of a benchmark research vessel propeller. Ocean Engineering, 211, 107549.

[15]   Sheldahl, R. E., & Klimas, P. C. (1981). Aerodynamic characteristics of seven symmetrical airfoil sections through 180-degree angle of attack for use in aerodynamic analysis of vertical axis wind turbines (No. SAND-80-2114). Sandia National Labs, NM (USA).

[16]   Celik, I. B., Ghia, U., Roache, P. J., & Freitas, C. J. (2008). Procedure for estimation and reporting of uncertainty due to discretization in CFD applications. Journal of fluids Engineering-Transactions of the ASME, 130(7).